

INTRACLUSTER MEDIUM REHEATING BY RELATIVISTIC JETS.

MANEL PERUCHO, VICENT QUILIS AND JOSÉ MARÍA MARTÍ

Departament d'Astronomia i Astrofísica. Universitat de València. C/ Dr. Moliner 50, 46100 Burjassot (València), Spain
Draft version October 14, 2011

ABSTRACT

Galactic jets are powerful energy sources reheating the intra-cluster medium in galaxy clusters. Their crucial role in the cosmic puzzle, motivated by observations, has been established by a great number of numerical simulations missing the relativistic nature of these jets. We present the first relativistic simulations of the very long term evolution of realistic galactic jets. Unexpectedly, our results show no buoyant bubbles, but large cocoon regions compatible with the observed X-ray cavities. The reheating is more efficient and faster than in previous scenarios, and it is produced by the shock wave driven by the jet, that survives for several hundreds of Myrs. Therefore, the X-ray cavities in clusters produced by powerful relativistic jets would remain confined by weak shocks for extremely long periods, whose detection could be an observational challenge.

Subject headings: Galaxies: active — Galaxies: jets — Hydrodynamics — Shock-waves — Relativistic processes — X-rays: galaxies: clusters

1. INTRODUCTION

Galaxy clusters are formed by dark matter and gas. This last component appears in the form of galaxies and a diffuse hot gas filling the space amid them – the intra cluster medium (ICM). The basic laws of physics predict that huge amounts of this gaseous component – ICM – should cool due to bremsstrahlung radiation and fall onto the central galaxies in the clusters. These flows of cold gas would eventually be intimately related with crucial processes in the galaxy formation, like for instance, the star formation history in galaxies. However, these flows – the so called cooling flows – have not been observed in most of the clusters, or when observed, they are not as important as expected. In order to reconcile the theoretical results with the observations, several physical mechanisms have been invoked, being the most widely accepted, the reheating of the ICM by the Active Galactic Nuclei (AGN) feedback (Fabian 1994; McNamara & Nulsen 2007).

The state-of-the-art picture of the AGN feedback is underpinned on the idea that galactic jets can transport energy from the very center of the galaxy out to the cluster scales. These energy injections would inflate bubbles whose evolution would have two well differentiated phases: first, a shock dominated supersonic phase, followed by a second subsonic phase when the bubbles inflated by the jets would be buoyant in the ICM (Cattaneo et al. 2009).

The buoyant bubbles are unstable, due to Rayleigh-Taylor and Kelvin-Helmoltz instabilities, when interacting with the surrounding ICM, leading to a mixture of the hot gas locked in the bubble with the environment. Besides, an additional mixing is produced at the turbulent wake created by the buoyant bubbles rising up in the cluster potential well. All this mixing produces a net gain of internal energy of the ICM resulting in an efficient feedback mechanism able to stop or delay the cooling flows (see, e.g., Churazov et al. 2001; Quilis, Bower & Balogh 2001; Brüggen & Kaiser 2002; Churazov et al. 2002; Ruszkowski & Begelman

2002; Birzan et al. 2004; Dalla Vecchia et al. 2004; Roychowdhury et al. 2004; Brighenti & Mathews 2006; Sternberg & Soker 2008; De Young 2010). The idea that the radio lobes reach pressure equilibrium with their environment in a relatively short time supports the model of buoyant motion of the bubbles inflated by the jets (McNamara & Nulsen 2007). However, the observations of shocks in several sources like Hercules A (Nulsen et al. 2005), Hydra A (Simionescu et al. 2009), MS0735.6+7421 (McNamara et al. 2005) or HCG 62 (Gitti et al. 2010) may require to reconsider the relevance of the subsonic buoyant phase. Specially, when observational evidences (Kraft et al. 2007; Croston et al. 2007) and numerical simulations (Perucho & Martí 2007; Bordas, Bosch-Ramon & Perucho 2011) have shown that even very modest energy injections – low-power FRI jets – with ages $\simeq 10^7$ yrs still present relatively strong shocks.

The AGN feedback scenario has mainly been established by a great number of numerical simulations studying the long term evolution of jets (e.g., Churazov et al. 2001; Quilis, Bower & Balogh 2001; Brüggen & Kaiser 2002; Reynolds, Heinz & Begelman 2002; Omma et al. 2004; Omma & Binney 2004; Zanni et al. 2005; Brighenti & Mathews 2006; Vernaleo & Reynolds 2006; Cattaneo & Teyssier 2007; Vernaleo & Reynolds 2007; Brüggen et al. 2007; Binney, Alouani Bibi & Omma 2007; Brüggen et al. 2009; O'Neill & Jones 2010). In these works, the input of jets was modeled injecting mass, momentum and energy in a few computational cells with a huge size (for jet scales) and with low (i.e., non-relativistic) flow velocities and temperatures imposed by the Newtonian approach. These inherent constraints could have direct implications on the evolution of the simulated jets since, in order to match the typical momentum and energy fluxes, the jets are set up with unrealistic opening angles, radii, and flux masses when compared with observations. This could be the reason leading, in general, to the formation of weak shock waves (with Mach numbers $M_s \leq 5$) and, as a consequence, to an early transition to the subsonic

phase in almost all the simulations performed until now.

In this paper we present, for the first time, the results of a set of very long term axisymmetric FRII-like jet simulations evolved using a fully relativistic description of the fluid dynamics and thermodynamics, also including a relativistic equation of state. Our approach allows the simulations to reconcile the inferred momentum and energy fluxes of observed jets with reasonable values of the jet flow velocities, radii, opening angles and mass fluxes. The use of the relativistic equation of state accounts consistently for the relativistic character of electrons in the jet and, to a less extent, in the cocoon, and the non-relativistic behaviour of protons. Also our relativistic models correctly describe, by construction, the deceleration of the relativistic flow and the internal and kinetic energy fluxes across the jet terminal shock, that govern the effective energy flux into the cocoon.

2. SIMULATIONS

2.1. Setup

We simulate the jets as energy injections in a realistic environment at a distance as close as 1 kpc to the nucleus of the source and follow the evolution up to several hundreds of kiloparsecs. The jets are injected with an initial radius of 100 pc with flow velocities ranging from $v_j = 0.9c$ to $v_j = 0.99c$, and typical density ratio between the jet material and environment of $\rho_j/\rho_a = 5 \times 10^{-4}$. The jets are fed by the injection of energy during 50 Myrs (16 Myrs in one model), when they are switched off so as to mimic a duty cycle event. The total injected energies range from 3×10^{59} to 10^{61} erg, depending on the jet model (see solid-black lines in Fig. 3). Our best numerical resolution is 50×50 parsecs. A complete list of all relevant parameters of the simulations is described in Table 1.

All the performed simulations are 2D axisymmetric. The jets are injected in a computational domain filled with an ambient in hydrostatic equilibrium, which is formed by primordial gas with a King-like density profile considering the elliptical galaxy – origin of the jet – and the galaxy cluster. The density profile parameters have been fixed by fitting the X-ray data of the source 3C 31 (Hardcastle et al. 2002). The ambient density at the injection point is 0.1 particles per cubic centimetre. The dark matter halo follows a NFW density profile (Navarro, Frenk & White 1997). All these parameters represent a moderate size galaxy cluster with mass $10^{14} M_\odot$ and ~ 1 Mpc virial radius.

The numerical grid is structured as follows: in the radial direction, a grid with the finest resolution extends up to 50 kpc (Model J1) or 100 kpc (Models J2, J3, J4). An extended grid with decreasing resolution was added up to 1 Mpc. The time-step during the first part of the simulations, when the jet is still active, was 50 to 100 years. The boundary conditions in the simulations are reflection at the jet base, to mimic the presence of a counter-jet, reflection at the jet axis and outflow at the end of the grid in the axial and radial directions.

The simulations presented in this paper use the finite-volume code *Ratpenat*, which solves the equations of relativistic hydrodynamics in conservation form using high-resolution-shock-capturing methods. *Ratpenat* is a hybrid parallel code – MPI + OpenMP – extensively and

intensively tested (e.g., Perucho et al. 2010). The code includes the Synge equation of state (Synge 1957) with two populations of particles, namely, leptons (electrons and positrons) and baryons (protons). In these simulations, cooling has not been taken into account, as the typical cooling times in the environment are long compared to the simulation times (see Figure 10 in Hardcastle et al. 2002).

2.2. Results

The dynamics of the system is dominated by the jet active phase, where jet head velocities range from $0.01c$ to $0.06c$, consistently with different estimates of the advance velocities of active radio sources ($0.02 - 0.2c$) (Carilli & Barthel 1996), implying Mach numbers between 10 (J3) and 30 (J2). The evolution of the supersonic jet generates a characteristic morphology: i) a bow-shock that acts on the ambient medium, ii) a terminal or reverse shock at the head of the jet where the flow is decelerated and iii) the cocoon inflated by the shocked jet particles and polluted with shocked ICM stirred via instabilities arising at the contact discontinuity between both media, typically hotter and underdense compared with the ambient. After the switching off, due to the short time scales needed by the relativistic fluid to reach the jet terminal shock, the jet head velocities quickly drop to values $\sim 10^{-3}c$ making the bow-shock to approach sphericity very fast. During this phase, the Mach numbers of the bow-shock fall from ~ 10 to values between 1 and 2.

Figure 1 shows four snapshots of model J2 at representative phases of its evolution (see Sec. 3.1). The jet is seen in the second panel (also in the first one although less clearly due to the small size of the system) as a blue or green line on the axis in the density and temperature frames, respectively. The terminal shock at the head of the jet is also seen in this panel, specially in the temperature distribution, as the dark red (saturated) region at the end of the jet. After the jet switch-off, the channel opened by the jet is still seen on the axis in the third and fourth frames although the jet terminal shock has already disappeared. In the four panels, the cocoon is the bluish turbulent region in the density frames (reddish region in the temperature ones), whereas the shocked ambient medium fills the region between the cocoon and the bow shock (yellow/orange/red region in the density frames; light blue region in the temperature frames). The density is low (i.e., smaller than the density in the original unperturbed medium) in the cocoon and high in the shocked ambient region.

The key features that differentiate the simulated jets are the injection power and the duration of the active phase. The location of the bow shock at a given time is largely dependent on these parameters and hence the distance at which the energy is deposited. The morphology of the cocoon also changes for the different models, with the most powerful jet (J2) creating a large cavity and the less powerful one (J3) having its particles distributed closer to the source. The gross properties of models J1 and J4, with the same power and different composition, are very similar.

In all the cases studied, the late stages of the simulations show a cocoon composed by jet and ICM shocked particles completely mixed, forming a low density region

TABLE 1
PARAMETERS OF THE SIMULATED JETS

Model	Velocity [c]	Density [g/cm ³]	X_e	L_k [erg/s]	max. resol. [pc/cell]	t_{off} [Myrs]
J1	0.9	8.3×10^{-29}	1.0	10^{45}	50	50
J2	0.984	8.3×10^{-29}	1.0	10^{46}	100	16
J3	0.9	8.3×10^{-30}	1.0	10^{44}	100	50
J4	0.9	8.3×10^{-29}	0.5	10^{45}	100	50

From left to right the columns give the model, the injection velocity, the injection density, the leptonic number, the jet power, the maximum resolution, and the switch-off time.

surrounded by the denser shocked ICM, with temperatures within the cocoon not larger than one order of magnitude those in the shocked medium. All these features postulate the cocoon as an excellent candidate precursor of the X-ray observed cavities. Surprisingly, in all our simulations, covering two orders of magnitude in jet power and a factor of 30 in total injected energy, the pressure jumps between the shocked and the unperturbed ICM persist along the whole simulation, and no buoyant stage is reached. Fig. 2 shows the X-ray emission obtained from one snapshot in simulation J2 compared to a real observation.

The minimum cooling times have been calculated at different times during the simulation to check the consistency of the results, taking into account that cooling has not been included. After the medium is perturbed by the jet, minimum cooling times are longer than the simulated ones by more than a factor 10 during the active phase, and by more than 100 or 1000 times the simulated time after the jet switch-off. Significant changes in the results presented in this work are thus not expected if the cooling terms are included.

3. DISCUSSION

3.1. Cavity evolution

The long-term evolution of the cocoons in our numerical simulations, within the shock dominated supersonic phase, can be interpreted as undertaking three stages: i) a short one-dimensional phase, in which the cocoon expansion is governed by the one-dimensional evolution of the jet (up to $t \approx 1.8$ Myrs in model J2); ii) a genuinely multidimensional phase in which the cocoon expansion is driven by a decelerating jet as a result of the multidimensional effects affecting the jet propagation, and iii) a Sedov phase (starting at $t = 16$ Myrs in model J2), in which the cocoons expand passively once the energy injection of the jet has ceased. In this last phase, the expansion on a density decreasing atmosphere is expected to produce a faster expansion of the cocoon (and consequently a faster pressure decrease) than in the pure Sedov case (constant ambient density). The first two phases are typical of the propagation of supersonic jets and are described in, e.g., Scheck et al. (2002). The third phase is new and follows from the jet switch-off.

Figure 1 shows four snapshots of model J2 at representative stages of its evolution: one-dimensional (first panel), multidimensional (second panel) and Sedov phases (third and fourth panels). In a homogeneous ambient, during the so-called one-dimensional phase, the jet propagates at its estimated one-dimensional speed (Martí et al. 1997). The propagation efficiency of the jet during this phase is maximum and the cocoon in-

flates at its smallest rate. In the present simulations, the evolution in a density decreasing atmosphere accelerates the jet propagation speed beyond the one-dimensional estimate and makes the cocoon expansion faster. The onset of the multidimensional phase is triggered by multidimensional, dynamical processes taking place close to the jet's head. During this phase, the generation of large vortices at the jet/shocked ambient interface (a pair of such vortices are seen at the jet's head in the density map of the second panel) decelerates the jet increasing the flux of jet material into the cocoon. As a result, the cocoon expands at a fast rate (helped also by the decreasing ambient density). Third and fourth panels in Fig. 1 are representative of the Sedov phase, once the jet has been switched-off. Consistently, the jet losses its hot-spot (the impact point of the jet on the ambient medium), still seen in the second panel, and the channel opened by the jet starts to be refilled. During this phase, the cocoon continues its expansion (at a smaller rate than in the previous phase since the injection of energy has ceased) and tends to sphericity (since there is no extra momentum transfer in the axial direction any longer).

The temperature is quite homogeneous within the cocoon, and almost constant with time as far as there is a continuous and constant matter and energy injection through the jet. Once the jet is switched-off, the cocoon starts to cool down (see the evolution of the cocoon temperature between the third and fourth panels).

At late stages, the velocity field in the cocoon is dominated by the overall cocoon expansion speed ($\leq 3 \times 10^{-3}$ c) and the turbulent motions on smaller scales, with local values of the order of 0.04 c.

Begelman-Cioffi's model (Begelman & Cioffi 1989) (BC) describes the expansion against a uniform ambient medium of the overpressured cocoons raised by the continuous injection of energy from a supersonic jet. In this model the axial expansion of the cocoon (i.e. along the jet) proceeds at the (constant) advance speed determined by the jet, whereas the sideways growth follows from the assumption of the evolution being mediated by a strong shock.

The long-term evolution of the cocoons in our numerical simulations can be consistently described within the so-called extended Begelman-Cioffi's model (Scheck et al. 2002; Perucho & Martí 2007) (eBC) that allows for a power-law dependence of the jet advance speed with time and a non-uniform ambient medium. In addition, the model can also describe the passive (supersonic) expansion of the cocoon once the jet has ceased its activity (Sedov phase).

In the eBC model, if the advance speed of the bow

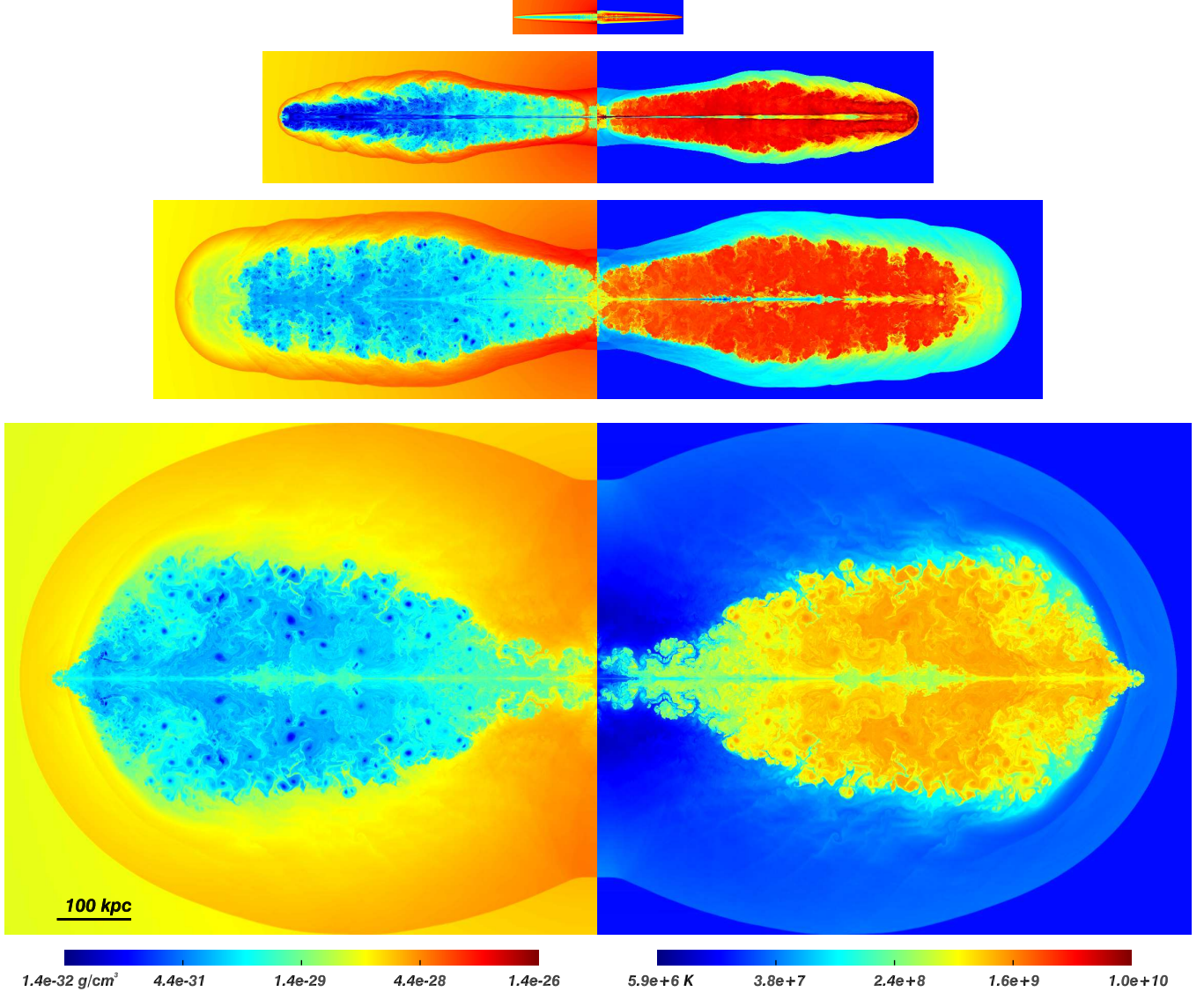


FIG. 1.— Maps of logarithms of rest-mass density (left) and temperature (right) for simulation J2 at times 1.1, 13.5, 34 and 180 Myrs. The figures show a mirrored image around the symmetry axis and plane in the simulation. The color-scale (in the online version only) of the temperature plot has been cut at 10^{10} K for the sake of clarity. Although the maxima in the first and second snapshots are 5×10^{10} K and 4.5×10^{11} K, these values are only reached in a very small region at the head of the jet (hotspots), which accordingly saturate the color-scale used.

shock along the axial direction, v_c , and the ambient density, ρ_a , follow the power laws $v_c \propto t^\alpha$, $\rho_a \propto r^\beta$, then, the cavity's transversal dimension, R_c , and pressure, P_c , follow

$$R_c \propto t^{\frac{2-\alpha}{4+\beta}}, \quad P_c \propto t^{\frac{2(\alpha-2)-\alpha(4+\beta)}{4+\beta}}. \quad (1)$$

These time dependencies are valid as far as there is a constant injection of energy in the cocoon. Once the jet is switched off (Sedov phase), the evolution follows

$$R_c \propto t^{\frac{1-\alpha}{4+\beta}}, \quad P_c \propto t^{\frac{2(\alpha-1)-(1+\alpha)(4+\beta)}{4+\beta}} \quad (2)$$

(the pure Sedov expansion phase is recovered when $\alpha = -3/5$ and $\beta = 0$, for which $R_c \propto t^{2/5}$, and $P_c \propto t^{-6/5}$).

Table 2 displays the parameters α (derived from the simulations) and β for the three phases of each simulation, and the corresponding exponents for the time de-

pendence of R_c and P_c both from the simulations and from the eBC model. According to the data displayed in this table, we can conclude that the eBC model describes consistently the long-term evolution of the cocoons along phases i) and ii). Concerning the Sedov phase, let us note first that our model produces a faster expansion (time exponent for R_c around $3/5$ instead of $2/5$) and a faster pressure decrease (time exponent for P_c around $-7/5$ instead of $-6/5$), as expected. However it must be noted that the exponents derived from the simulations reinforce this tendency. The discrepancies between the expected and the obtained time dependencies in this last phase have a clear dependence on jet power and could be a signature of the buoyant force acting on the (still supersonic) cavities.

TABLE 2
PARAMETERS FOR THE THREE STAGES OF THE EVOLUTION WITHIN EACH OF THE SIMULATIONS.

		1D phase				2D phase				Sedov phase			
		α	β	P_c	R_c	α	β	P_c	R_c	α	β	P_c	R_c
J1	Sim	0.07	-1.55	-1.58	0.75	-0.23	-0.52	-1.09	0.66	-0.74	-1.02	-1.70	0.90
	Model			-1.65	0.79			-1.05	0.64			-1.43	0.58
J2	Sim	0.27	-1.55	-1.67	0.67	-0.57	-0.52	-0.95	0.81	-0.83	-1.02	-1.67	0.72
	Model			-1.68	0.71			-0.91	0.74			-1.40	0.61
J3	Sim	0.13	-1.55	-1.55	0.67	-0.35	-0.52	-1.08	0.74	-0.60	-1.02	-2.16	1.00
	Model			-1.66	0.76			-1.00	0.68			-1.47	0.54

The parameters α and β are derived from the simulations (first two columns for each phase). The time dependence of R_c and P_c (third and fourth columns, respectively) is shown as obtained from the simulation and from the eBC model.

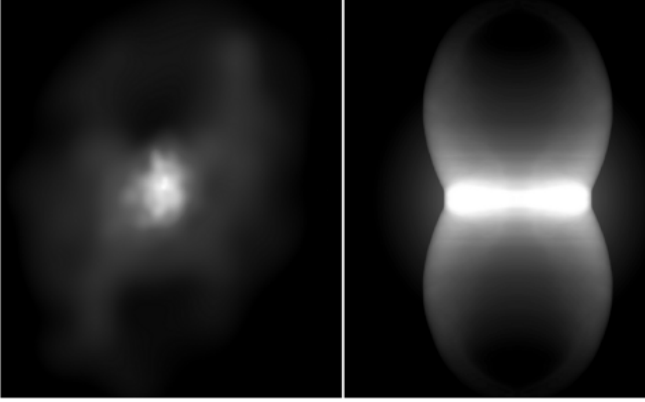


FIG. 2.— Qualitative comparison of an X-ray map of the cluster MS 0735.6+7421 (McNamara et al. 2005) (left, credit: X-ray image: NASA / CXC / Ohio U. / B.McNamara et al.; illustration: NASA / CXC / M.Weiss) and a synthetic X-ray luminosity map extracted from simulation J2 (right). Although this comparison must be taken with caution, the main features of both images seem to match remarkably well.

3.2. Heating of the ambient medium

The efficiency of the heating triggered by the bow shock is very high in two aspects, namely the amount of ambient medium heated per unit time and the amount of energy transferred to the ambient medium in the heating process. With respect to the first point, let us note that the heating front propagates through the ambient medium at the shock speed (a substantial fraction of the light speed during the first stages of evolution). As an example, the shock in model J2 has processed about $9.4 \times 10^4 \text{ kpc}^3$ by the end of the one-dimensional phase ($t \approx 1.8 \text{ Myrs}$), $1.1 \times 10^7 \text{ kpc}^3$ at the onset of the Sedov phase ($t \approx 16 \text{ Myrs}$), and 0.37 Mpc^3 at the end of the simulation ($t \approx 160 \text{ Myrs}$).

The transfer of energy to the ambient medium is also very efficient. Indeed, the energetic balance of our simulations (Fig. 3) shows that between 95% and 97% of the injected energy by the jet is instantaneously transferred to the ambient medium through shock-heating, mixing, and acceleration. The small residual is invested on gaining potential energy or kept by the jet particles. By the end of our simulations, between 10^{11} to $10^{12} M_\odot$ of ICM gas have been heated up by the shock, depending on the total energy injected during the active phase, in agreement with constraints imposed by observational data (McNamara & Nulsen 2007). Only a small fraction of the reheated ICM gas – from 0.1 to 1% – is mixed by

instabilities arising at the contact discontinuity between the shocked ambient and the shocked jet fluid. Therefore, the bulk of the heating comes from the action of the shock, being the mixing with the jet material negligible from the energetic point of view.

Figure 4 shows the energy per particle inside the shocked region versus time for all four simulations. The energy per particle, including the jet and ambient components, inside the bow-shock is always over 1 keV for J1, J2 and J4, whereas it falls below this value after $\simeq 10^8 \text{ yrs}$ in J3 case. Any effective reheating mechanism able to stop the cooling flows would require energies per particle $\sim 1 \text{ keV}$ (McNamara & Nulsen 2007). Figure 5 shows the average internal energy per unit volume versus distance to the source at different times, for the case of J2. The plot reveals where the energy is deposited. The values at small radii at the smaller times (mainly 1 and 15 Myr) are influenced by the elongated shape of the bow-shock. When the bow-shock becomes closer to sphericity at later times, the energy density has its maximum in a wide shell behind the shock-front. These facts confirm that the bow-shock dominates the energy deposition during the whole evolution. The heating of the cooling region ($\simeq 20 \text{ kpc}$, Hardcastle et al. 2002) is very fast ($< 1 \text{ Myr}$). It is also remarkable that, after 50 Myrs, the energy density falls below the original one. In the case of J2, the injection time was fixed to be 16 Myrs, implying that the simulation has been run for $\simeq 12$ times the active time. Taking into account that the heating mechanism is very fast and acts mainly at the bow-shock, as the shock propagates outwards, the central regions cool down due to expansion. This fast cooling is the reason why slower heating mechanisms are favoured in the literature (Omma & Binney 2004). Nevertheless, there are two aspects to be taken into account: 1) the gas in the inner region is still expanding, and 2) considering that this activity period has only implied the injection of $\simeq 2 \times 10^5 M_\odot$, which does not represent a large amount of material out of the total amount of matter and energy expected to be present in the surroundings of AGN. New periods of activity would be expected to occur more often than 16 Myrs every 180 Myrs (see, e.g., Fabian et al. 2006). We note that even short periods of activity ($< 1 \text{ Myr}$) with the same power, are enough to heat and empty the ambient inside the cooling region.

The moderate size galaxy cluster considered in our simulations, with mass $10^{14} M_\odot$ and 1 Mpc virial radius, does favour the persistence of the bow shock generated in the expansion of the cavities. However, a ten times more

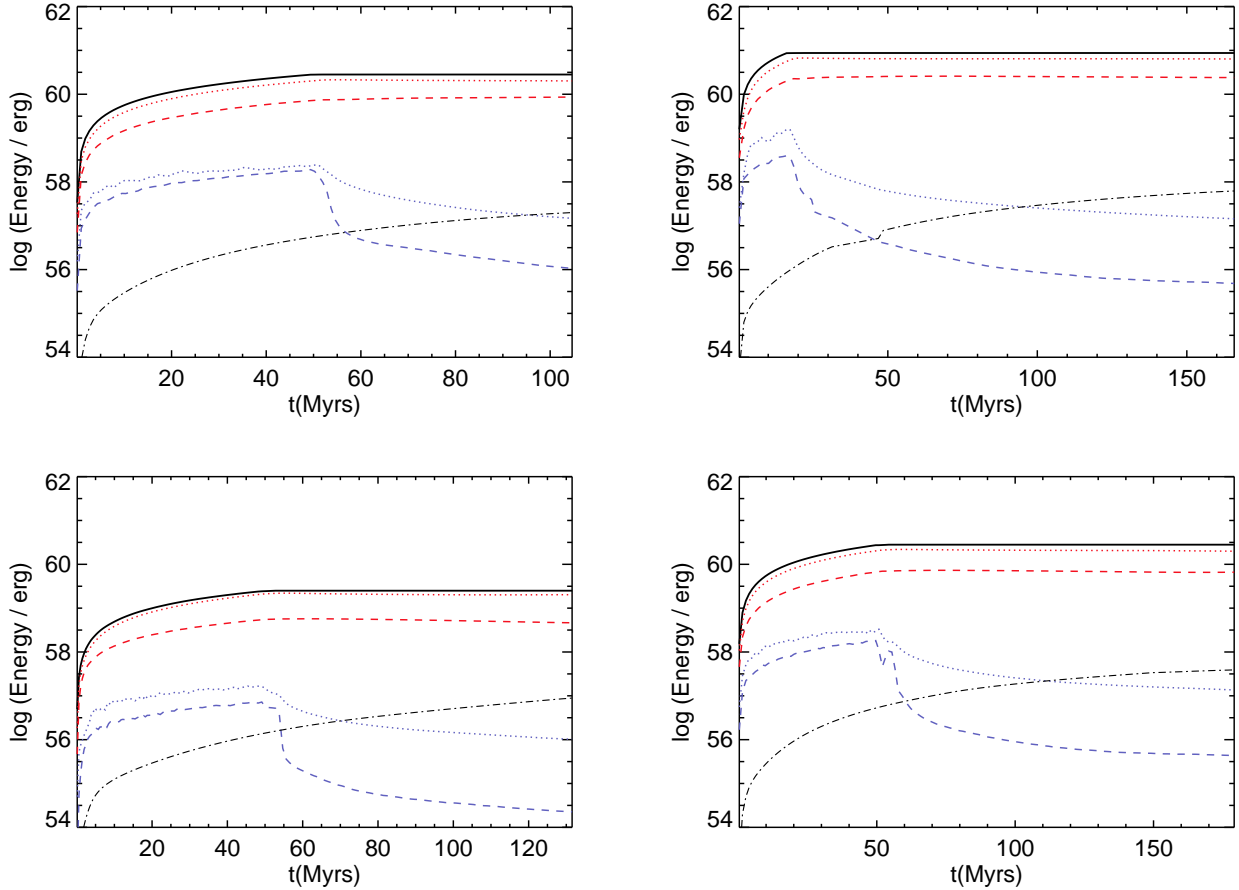


FIG. 3.— Logarithm of energy versus time for the four simulations. The top panels show the results for models J1 and J2, respectively, whereas the bottom panels show those for J3 and J4. The red-dotted lines (color only in the online version) and the red-dashed lines represent, respectively, the increase of internal and kinetic energy in the processed ambient medium. The blue lines, dotted and dashed, display the internal and kinetic energy of the jet material. The increase of potential energy is shown by the black dashed-dotted line. The upper thick black line is the total injected energy. These plots reveal that the jet material barely keeps a small fraction of its injected energy (less than 1%), which is mainly transferred to the ambient. After the switching off, the jet material keeps on transferring energy to the ambient via mixing, being this the explanation to the energy drop after this time. A tracer, evolved in the code as an additional conserved variable in the set of equations, allow us to accurately discriminate between jet and ambient material.

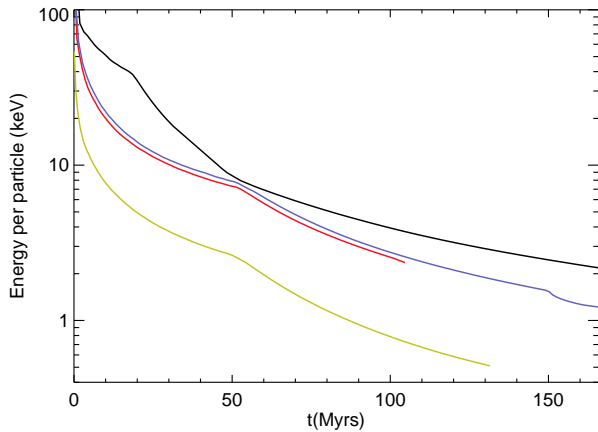


FIG. 4.— Energy per particle inside the bow-shock versus time for the four simulations. J1 is represented by red color, J2 by black, J3 by yellow, and J4 by blue (color only in the online version).

10 times larger will reduce the volume processed by the shock in the same factor or, equivalently, in roughly a factor of 2 per spatial dimension. Moreover large changes in the processed mass are not expected because of the denser ambient medium. Finally, the same amount of injected energy acting on a similar amount of particles would lead to similar values of energy per particle.

3.3. Jet/cavity energy balance

The energy injected by the jet is invested primarily in inflating the cavity against the ambient medium and heating the ambient gas remaining within it. Other contributions, like, e.g., the kinetic energy transferred to the ambient, the change in the potential gravitational energy of the pushed-aside material, and the energy kept by the jet particles, are neglected in the jet/cavity energy balance estimates in real sources. The energy invested in inflating the cavity is the pV expansion work exerted on the ambient. It is usually estimated from the volume of the cavity and the average pressure surrounding it. In the case of the cluster MS 0735.6+7421 (McNamara et al. 2005), where the cavities are roughly 200 kpc in diame-

massive cluster with an average density (and pressure)

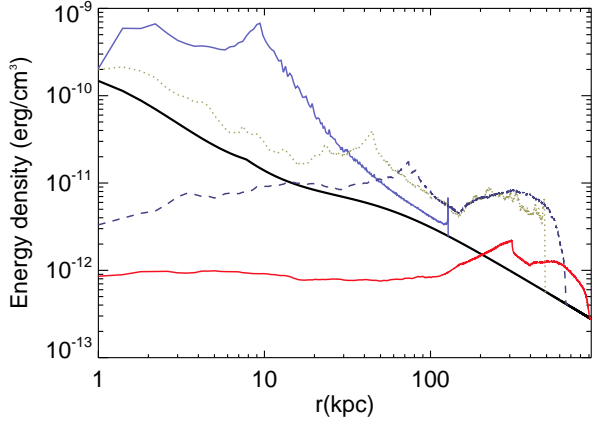


FIG. 5.— Average internal energy density versus radius from the nucleus for simulation J2, at different times. The blue-solid line is calculated at $t = 1$ Myr, the green-dotted line at $t = 15$ Myr, the blue-dashed line at $t = 50$ Myr, and the red-solid line at $t = 180$ Myr (color only in the online version).

ter and the surrounding pressure, 6×10^{-11} ergs/cm³, the work required to inflate each cavity against this pressure is $pV \approx 10^{61}$ ergs. The internal energy in the cavity, i.e., the second term in the jet/cavity energy balance, is usually estimated as being few times the pV term (3 times in the case of the MS 0735.6+7421 cluster).

Our simulations allow for a check of the hypothesis below the jet/cavity energy balance estimates summarized in the previous paragraph. First of all the results shown in Fig. 3 confirm that the kinetic energy in the ambient gas, the change in the potential gravitational energy, and the energy kept by the jet particles are negligible, contributing with less than 10% to the global energetics. Now, the expansion work of the cavity can be approximately accounted for through estimates of the cocoon volume and the average pressure of the original ambient medium swept by the jet. For the model J2 ($t = 180$ Myrs), the volume of the cocoon is $\approx 3.4 \times 10^7$ kpc³ (i.e., about 400 kpc of effective diameter), whereas the averaged pressure is $\approx 3 \times 10^{-13}$ erg/cm³ (200 times the pressure used in the MS 0735.6+7421 calculation). The resulting work is $pV \approx 3 \times 10^{59}$ ergs. Finally, the average internal energy density in the cavity is estimated to be 10^{-12} erg/cm³. With these numbers, the minimum total energy needed to inflate one of the cavities in simulation J2 results to be 1.3×10^{60} ergs, in good agreement with the total energy injected by the jet (5×10^{60} ergs), reflecting the consistency of our analysis. Finally, as a by-product, we note that our result confirms the factor of 3 between the internal energy stored in the cavity and the expansion work assumed in the case of the MS 0735.6+7421 cluster, but now under very different conditions: in a two orders of magnitude lighter cluster and for a total injected energy 10 times smaller.

3.4. Possible three-dimensional effects

We must make a final comment on the 2D nature of the simulations, for it could be seen as an important limitation in our conclusions. In the long term, the evolution of

the cavity is driven by its internal pressure, which i) depends basically of the total energy injected in the cocoon, and ii) tends to isotropize the cocoon on a characteristic time scale of its internal sound speed (of the same order or larger than the overall shock advance speed). Both aspects tend to reduce the importance of the early three-dimensional effects in the long term evolution of cavities making more reliable the conclusions derived from our present axisymmetric simulations. Moreover, the ambiguity in the initial condition parameter space for the jet and ambient could lead to results with larger dispersion than those arising from possible 3D effects.

4. CONCLUSIONS

We have presented the first simulations on the impact of relativistic AGN jets in the heating of the intracluster medium. Our simulations cover the longest spatial and temporal scales considered up to now and besides this, due to their relativistic character, also for the first time, allow for a consistent description of the jets (that have consistent values of the jet flow velocities, radii, opening angles and mass, momentum and energy fluxes) within the cluster heating scenario.

Our simulations show that heating by AGN jets is mainly driven by shock heating, resulting in a very fast and efficient process (more than 95% of the energy injected through the jets is transferred to the ambient). As a by-product, our simulations also show that although buoyant cavities could be the very final stage of radiogalactic relics, they are not the main actors in the ICM reheating.

As a result of our simulations, we suggest the idea that most of the observed X-ray cavities are confined by shock waves, very weak though. Although it can not be concluded that the presence of shock confined cavities implies the relativistic nature of jets, such shocks in our results last for much longer periods than in previous – Newtonian – works. The confirmation of the existence of such weak shock waves could be an observational challenge that would have crucial implications in our understanding of the galaxy formation and evolution paradigm.

Simulations were carried out using resources from the Spanish Supercomputing Network (RES). This Research Project has been supported by Spanish Ministerio de Ciencia e Innovación (grants AYA2010-21322-C03-01, AYA2010-21097-C03-01 and CONSOLIDER2007-00050) and by the Generalitat Valenciana (grant PROMETEO-2009-103). MP acknowledges support from MICINN through a “Juan de la Cierva” contract. We thank B.R. McNamara for providing an X-ray image of the cluster MS 0735.6+7421. The authors thank the anonymous referee for constructive criticism and comments that have improved the manuscript.

REFERENCES

- Begelman, M.C., Cioffi, D.F., 1989, *ApJ*, 345, L21
- Binney, J., Alouani Bibi, F., Omma, H., 2007, *MNRAS*, 377, 142
- Birzan, L., Rafferty, D.A., McNamara, B.R., Wise, M.W., Nulsen, P.E.J., 2004, *ApJ*, 607, 800
- Bordas, P., Bosch-Ramon, V., Perucho, M., 2011, *MNRAS*, 412, 1229
- Brighenti, F., Mathews, W.G., 2006, *ApJ*, 643, 120
- Brüggen, M., Kaiser, C.R., 2002, *Nature*, 418, 301
- Brüggen, M., Heinz, S., Roediger, E., Ruszkowski, M., Simionescu, A., 2007, *MNRAS*, 380, L67
- Brüggen, M., Scannapieco, E., Heinz, S., 2009, *MNRAS*, 395, 2210
- Carilli, C.L., Barthel, P.D., 1996, *A&A Rev.*, 7, 1
- Cattaneo, A., Teyssier, R., 2007, *MNRAS*, 376, 1547
- Cattaneo, A., Faber, S.M., Binney, J., *et al.*, 2009, *Nature*, 460, 213
- Churazov, E., Brüggen, M., Kaiser, C.R., Böhringer, H., Forman, W., 2001, *ApJ*, 554, 261
- Churazov, E., Sunyaev, R., Forman, W., Böhringer, H., 2002, *MNRAS*, 332, 729
- Croston, J.H., Kraft R.P., Hardcastle M.J., 2007, *ApJ*, 660, 191
- Dalla Vecchia, C., Bower, R.G., Theuns, T., Balogh, M.L., Mazzotta, P., Frenk, C.S., 2004, *MNRAS*, 355, 995
- De Young, D.S., 2010, *ApJ*, 710, 743
- Fabian, A.C., 1994, *ARA&A*, 32, 277
- Fabian, A.C., Sanders, J.S., Taylor, G.B., Allen, S.W., Crawford, C.S., Johnstone, R.M., Iwasawa, K., 2006, *MNRAS*, 366, 417
- Gitti, M., O'Sullivan, E., Giacintucci, S., David, L.P., Vrtillek, Jan, Raychaudhury, S., Nulsen, P.E.J., 2010, *ApJ*, 714, 758
- Hardcastle M. J., Worrall D. M., Birkinshaw, M., Laing, R. A., Bridle, A. H. 2002, *MNRAS*, 334, 182
- Kraft, R.P., Nulsen, P.E.J., Birkinshaw, M., 2007, *ApJ*, 665, 1129
- Martí, J.M., Müller, E., Font, J.A., Ibañez, J.M., Marquina, A., 1997, *ApJ*, 479, 151
- McNamara, B.R., Nulsen, P.E.J. 2007, *ARA&A*, 45, 117
- McNamara, B.R., Nulsen, P.E.J., Wise, M.W. *et al.*, 2005, *Nature*, 433, 45
- Navarro, J.F., Frenk, C.S., White, S.D.M., 1997, *ApJ*, 490, 493
- Nulsen, P.E.J., Hambrick, D.C., McNamara, B.R. *et al.*, 2005, *ApJ*, 625, L9
- Omma, H., Binney, J., Bryan, G., Slyz, A., 2004, *MNRAS*, 348, 1105
- Omma, H., Binney, J., 2004, *MNRAS*, 350, L13
- O'Neill, S.M., Jones, T.W., 2010, *ApJ*, 710, 180
- Perucho, M., Martí, J.M., 2007, *MNRAS*, 382, 526
- Perucho, M., Martí, J.M., Cela, J.M., Hanasz, M., de la Cruz, R., Rubio, F., 2010, *A&A*, 519, A41
- Quilis, V., Bower, R.G., Balogh, M.L., 2001, *MNRAS*, 328, 1091
- Reynolds, C.S., Heinz, S., Begelman, M.C., 2002, *MNRAS*, 332, 271
- Roychowdhury, S., Ruszkowski, M., Nath, B.B., Begelman, M.C., 2004, *ApJ*, 615, 681
- Ruszkowski, M., Begelman, M.C., 2002, *ApJ*, 581, 223
- Scheck L., Aloy, M.A., Martí, J.M., Gómez, J.L., Müller, E., 2002, *MNRAS*, 331, 615
- Simionescu, A., Roediger, E., Nulsen, P.E.J. *et al.* 2009, *A&A*, 495, 721
- Sternberg, A., Soker, N., 2008, *MNRAS*, 389, L13
- Synge, J.L., 1957, *The Relativistic Gas*. North-Holland publishing Company, Amsterdam
- Vernaleo, J.C., Reynolds, C.S., 2006, *ApJ*, 645, 83
- Vernaleo, J.C., Reynolds, C.S., 2007, *ApJ*, 671, 171
- Zanni, C., Murante, G., Bodo, G., Massaglia, S., Rossi, P., Ferrari, A., 2005, *A&A*, 429, 399